29th AIAA Applied Aerodynamics Conference
27 - 30 June 2011, Honolulu, Hawaii

AIAA 2011-3809

Shape Change of the Upper Surface of an Airfoil by Macro Fiber Composite Actuators

Marco Debiasi[1] and Yann Bouremel[2]
Temasek Laboratories, National University of Singapore, Singapore, 117411

Khoo Hock Hee[3] and Luo Siao Chung[4]
Department of Mechanical Engineering, National University of Singapore, Singapore, 117576

and

Elvin Tan Zhiwei[5]
School of Mechanical & Aerospace Engineering, Nanyang Technological University, Singapore, 639798

Macro fiber composite actuators are used to displace inward or outward the upper surface of a NACA 4415 airfoil model. In the design discussed, these thin and light piezoelectric actuators are bonded to the inside and become an integral part of the skin of the upper-surface. Still-air and wind-tunnel measurements in different flow regimes were performed to assess the characteristics of static changes of the shape of the upper surface. The results obtained can be used to design a wing with morphing upper surfaces for improved aerodynamics, for maneuvering without ailerons, or for active control of the flow over the wing.

Nomenclature

c	=	model chord
C_D	=	drag coefficient
C_L	=	lift coefficient
Re_c	=	Reynolds number based on the chord
s	=	model span (width)
U	=	flow velocity
x	=	streamwise coordinate
y	=	spanwise coordinate
z	=	normal coordinate

Greek letters

α	=	angle of attack of the airfoil
ω_y	=	vorticity along y

Symbols

∞	=	freestream conditions

[1] Senior Research Scientist, Temasek Laboratories, National University of Singapore, Singapore, Member AIAA.
[2] Research Scientist, Temasek Laboratories, National University of Singapore, Singapore.
[3] Graduate Student, Department of Mechanical Engineering, National University of Singapore, Singapore.
[4] Associate Professor, Department of Mechanical Engineering, National University of Singapore, Singapore.
[5] Graduate Student, School of Mechanical & Aerospace Engineering, Nanyang Technological University, Singapore.

I. Introduction

THE ability to change the shape of a wing allows adapting it to different flight conditions. Through evolution, birds, bats, and insects have developed wings capable of dramatic and continuous morphing not only for generating the lift required to stay aloft, but also to propel themselves in the air and to perform controlled maneuvers. To a smaller extent the wings of aircraft can also achieve discrete changes of their shape by using ailerons, flaps, and slats or by modifying their sweep, dihedral, or incidence angle. Thus much research is devoted to understand and optimize more extensive types of wing morphing for improving the aircraft performance.[1-6] However, extensive wing morphing poses significant design challenges and requires complex mechanical structures and actuators. By contrast limited but continuous morphing of a wing can be often sufficient for the needs of flight (as shown by the minimal movements of the wings of various birds in some flight conditions). At high-subsonic speed the selective displacement of an airfoil upper surface by less than 0.5 % of its chord is sufficient to introduce changes of the pressure distribution useful for tailoring the lift and drag coefficients.[7] This can be used to optimize the performance of an airfoil around a design point, for instance at cruise conditions. Asymmetric changes in the left and right wing can also be used to maneuver an aircraft without using ailerons. Larger displacements would be required at lower speed, but still within some few percent of a wing's chord. Furthermore, limited shape changes appear more feasible for actuation at high frequencies.[8] This can be exploited to actively control some undesirable phenomena of the wings like flow separation[9-11] and aeroelastic oscillations.[12-14]

A major difficulty in implementing wing morphing is represented by the size, weigh, complexity, and power[15] demanded by the appropriate actuators (hydraulic, pneumatic, electric motors, or even some smart materials like shape-memory alloys). From a system-integration point of view the performance increase offered by the morphing must out-weight its associated penalties. In this respect, limited morphing is also appealing as it may offer useful aerodynamic advantages with small, light, simple, and power-saving actuators.

The macro fiber composite (MFC) actuators, originally developed at NASA, belong to this category and seem promising for implementing different types of wing morphing, especially if limited shape changes are required. These thin, light, and flexible piezoelectric actuators, Fig. 1, consist of rectangular piezo-ceramic rods sandwiched between layers of adhesive and electroded polyimide film which contains interdigitated electrodes that transfer the applied voltage directly to the rods. When embedded in a surface or attached to flexible structures, the MFCs provide distributed deflection and vibration control. They can also be used as sensors to measure the structural strain under applied loads.

Some studies have explored the use of such actuators to change or control the shape of aerodynamic bodies. Munday et al. used THUNDER actuators (a predecessor of the MFC type, also developed at NASA) to increase the lift of an airfoil.[9-11] Their morphing airfoil model is based on a prototype made by Pinkerton and Moses.[16] Static and dynamic morphing tests were conducted at angles of attack from 0° to 9° at low Reynolds numbers of $2.5 \cdot 10^4$ and $5 \cdot 10^4$. Static morphing shows modest aerodynamic benefits with best increase of the *L/D* ratio of about 2%. However, dynamic morphing significantly reduces the size of flow separation therefore greatly increasing the *L/D* ratio. Bilgen et al. investigated the use of MFCs to change the wing camber for roll and pitch control of a remotely piloted micro-air-vehicle (MAV).[17] The MAV was flown successfully and demonstrated sufficient roll control in flight as well as in the wind tunnel. It survived numerous crashes proving the durability of MFCs. More recently Bilgen et al. investigated the use of MFCs to change the chamber of a symmetric airfoil.[18] Moses et al. studied MFC actuators as a means for reducing buffeting loads on a twin-tail fighter aircraft flying at high angles of attack.[19] Wind-tunnel tests with open and closed-loop buffet alleviation have shown buffeting reductions of over 80%.

The main scope of this project is to explore the use of MFC actuators integrated to the upper skin of a wing for changing the shape of its upper surface to the degree required for tailoring the wing's performance. To some extent this work parallels those of Munday et al. However the actuators used in this case are more advanced. Also, their integration in the wing structure is simpler and requires negligible space and minimal weight which are very desirable characteristics for practical implementation in aircraft.

II. Experimental Setup

A prototype airfoil model has been fabricated for testing the feasibility of shape changes by MFC actuators, Fig. 2a). Although not originally designed for aerodynamic testing, this model has also been used for preliminary wind-tunnel measurements of the aerodynamic effects of the shape changes. The geometry of the airfoil without MFC actuation is close to that of the NACA 4415 type. The model's chord *c* is 150 mm and its span *s* is 158 mm. The upper skin of the model is made of a 0.1 mm-thick stainless-steel foil to the inner side of which two MFC patches (Smart Material M-8557-P1) have been bonded, Fig. 2b). When a positive voltage is applied to the MFCs the skin

deflects inward, whereas it deflects outward when a negative voltage is applied, Fig. 3. The displacement causes the skin to have a small variation in the longitudinal direction which is accommodated by allowing it to slide in a thin pocket at the trailing edge.

The MFC actuators are driven by a Smart Material HVA 1500/50-2 high-voltage amplifier which is designed to supply a number of different piezo-actuators. This unit has a voltage gain of 200 V / V and a signal bandwidth from DC to 10 kHz depending on the load capacitance. It accepts input voltages in the range from -2.5 to 7.5 V which are amplified to values of -500V to 1500V, the voltage range of the MFC actuators.

The aerodynamic characteristics of the model have been tested in the small, open-loop, subsonic wind tunnel of the NUS Temasek Laboratories, Fig. 4. The range of the wind-tunnel freestream velocity U_∞ is 2 to 35 m/s. Square test sections with width and height of 160 mm and different lengths can be connected to the exit of the wind tunnel's nozzle which has a 9.8:1 contraction ratio. The turbulence intensity level of the wind-tunnel freestream is less than 0.25%. The leading edge of the model was located 200 mm downstream of the nozzle. In this location the boundary-layer thickness of the empty test section is less than 3 mm for values of U_∞ between 10 to 20 m/s. The nominal velocity of the flow upstream of the model was obtained by measuring its total pressure with a pitot intake upstream of the nozzle (and downstream of the settling chamber meshes) and its static pressure with a tap located in the wall of the test section 120 mm downstream of the nozzle. The total and static pressure ports were connected to an Extech HD350 digital anemometer. This arrangement permitted controlling and maintaining the flow velocity within ± 0.1 m/s.

The model was mounted on a turntable incorporating a balance. The turntable allows precise positioning (within ±0.2°) of the angle of attack α of the model. The balance consists of a Gamma ATI SI-65-5 piezoelectric gauge. This unit can measure the forces and the moments along three perpendicular axes. We used two axes aligned with the longitudinal and normal directions of the wind tunnel to measure the drag and the lift forces generated by the model. The third axis, coinciding with the axis of rotation of the turntable and aligned in the spanwise direction, passed through the airfoil mid-chord point (c/2) and was used to measure the pitching moment. The range (and accuracy) of the measured forces and moment are 65 (±1/80) N and 5 ($\pm 8 \cdot 10^{-4}$) Nm, respectively. For each measurement, 2048 samples of the voltage signals of the forces and moment were acquired at 2 kHz, low-pass filtered at 10 Hz in order to remove the effect of small vibrations induced by the flow, and then converted to physical values before averaging. Based on the angle of attack, the pitching moment about c/4 was calculated from the corresponding values of the lift, drag, and pitching moment about c/2. The maximum error for these quantities is 5%.

Flow-field velocity measurements were obtained by using a two-velocity-component particle image velocimetry (PIV) system. The flow was uniformly seeded upstream of the wind-tunnel air intake with olive oil particles from a Dantec 10F03 seeding generator. Droplets were produced in the average size Sauter mean diameter (SMD) 2-5 μm whose reflections correspond to no more than 3 pixels in the captured images which allows a good resolution of the particle displacement when cross correlation methods are adopted. A dual-head Litron DualPower 200-15 Nd:YAG laser operating at the second harmonic (532 nm) at approximately 150 mJ per pulse was used in conjunction with sheet-forming optics to form a thin sheet (~ 1 mm) on the x-z plane passing through the centerline of the test section. The images were acquired using double frame mode by a 2048 × 2048 pixels HiSense 620 camera with a Zeiss 50 mm f/2.0 macro lens (216 × 216 mm field of view). The resulting resolution is approximately 105 μm per pixel. The camera viewed the streamwise laser sheet orthogonally over the entire field of view. To retain a good resolution of the flow particles close to the upper surface of the model, a 527 to 537 nm band-pass optical filter was placed in front of the lens whereas the surface of the model exposed to the laser sheet was sprayed with clear acrylic paint containing rhodamine 6G (which fluoresces close to 566 nm when excited by 532 nm light). A computer with dual Intel Core processors was used for data acquisition. The acquired frames were divided into 16 × 16 pixel interrogation windows which contain at least 3 seeding particles each. Based on the flow velocity and the size of the interrogation area, the time separation between the two laser flashes (double frame mode) was set at 26 μs such that the maximum displacement of a particle is no more than 25% of the interrogation size which is the optimum displacement for the Dantec software to calculate accurately the particle velocity. For each frame, subregions were adaptatively cross-correlated using multi-pass processing with a final 50% overlap that gives a final interrogation area of 8 × 8 pixels after processing. The resulting vector fields were post-processed to remove remaining spurious vectors. This arrangement gives a velocity vector grid of 255 × 255 points which translates to velocity vectors separated by about 0.84 mm over the field of view. For each acquisition 200 velocity-vector images were taken for statistical averaging at a trigger rate of 6 Hz.

III. Results

Figure 5 shows lateral-view pictures of the model changing the shape of the upper surface with static actuation in still air. Figure 5a) is the model without actuation which has a shape similar to the NACA 4415 airfoil. Figure 5b) shows the effect of actuation at the minimum voltage of -500 V which produces a maximum outward displacement of about 3 mm (corresponding to 0.02 c) close to $c/2$. Increasing the voltage to the maximum value of 1500 V, Fig. 5c), produces a 5 mm inward displacement (corresponding to 0.03 c) at about the same location. Intermediate displacements between those of Figs. 5b) and 5c) are obtained for voltages between the minimum and maximum values above. In any case, little change of the shape of the upper surface is observed closer to the leading edge where the skin is rigidly connected to the model structure.

Wind-tunnel tests were performed at freestream velocities up to 20 m/s for values of the angle of attack ranging between -10° to 24°. In this range of velocities and angles of attack the upper skin of the model did not exhibit any vibration or anomalous deformation both without actuation and with actuation from the minimum to the maximum voltages. The response of the skin to actuation was comparable to that observed in still air.

Figure 6 compares the lift and drag coefficients of the non-actuated model to those of the NACA 4415 airfoil measured by Jacobs and Pinkerton.[20] The data, obtained at U_∞ = 15 m/s for α ranging between -6° to 14°, are not corrected for the effects of tunnel blockage. Larger values of the angle of attack are not considered since these would be significantly affected by the blockage of the model (whose chord is comparable to the height of the wind-tunnel test section). At this velocity the Reynolds number based on the chord of the model is about 150,000 and thus the flow around the model is laminar. Our data compare reasonably well with the NACA data even if the shape of our model is not exactly the same as the one of the NACA 4415 airfoil and the flow regime of the NACA experiments is turbulent ($Re_c > 3 \cdot 10^6$).

For the same conditions Fig. 7 compares the aerodynamic characteristics of the airfoil model without and with actuation. Since this model was originally designed to verify the feasibility of the shaping technique without any optimization of its aerodynamic shape, we did not expect to observe any performance increase with actuation. With maximum inward displacement the airfoil flattens and we would expect a lower lift coefficient. Consistently, Fig. 7a) shows that actuation at 1500 V has a slightly lower lift coefficient than the non-actuated case for $\alpha < 0°$ and for $\alpha > 6°$. We were hoping to observe the opposite with the maximum outward displacement, but the same figure indicates that the lift coefficient at -500 V is lower than the non-actuated case at least up to $\alpha = 8°$. Above this angle the lift coefficient sharply increases and becomes comparable to that of the non-actuated model. A similar change is also observed for the drag coefficient at -500 V which increases with α up to 8° after which it shifts to levels comparable to the non-actuated case, Fig. 7b). This unusual feature was verified by repeating our measurements several times. On the contrary, the drag coefficient with inward displacement at 1500 V is somewhat lower than the non-actuated case up to $\alpha = 6°$ after which it becomes slightly higher. Figure 7c) shows the corresponding drag polars. Interestingly, for C_L lower than 1 the inward displacement appears to offer a slight performance advantage by virtue of its lower drag over the non-actuated shape. However its performance rapidly degrades for larger values of C_L. Thus the non-actuated shape or possibly a shape with a slight outward displacement should be used to maintain optimal performance with C_L larger than 1. Figure 7d) shows the pitching moment coefficients about $c/4$. In the explored range of angles of attack the pitching moment with outward skin displacement is comparable to the non-actuated case but it exhibits a sudden change of values between $\alpha = 8°$ and 10° which corresponds to those observed for the lift and drag coefficient curves. In contrast, the moment with inward displacement is appreciably lower than the non-actuated case.

The data in Fig. 7 show that, in principle, the shaping of a surface by MFC actuators can be useful for tailoring the aerodynamic performance of an airfoil. In particular this technique could be very beneficial to broaden and stabilize the useful aerodynamic envelope of high-performance airfoils that quickly deteriorate their characteristics at off-design conditions (e.g. some Liebeck airfoils).

In order to clarify the unusual change between $\alpha = 8°$ and 10° for the coefficients obtained with actuation at -500 V, we used PIV to explore the flow fields above the model in these conditions. The results in Figs. 8 and 9 comprise two sets of data. The color fields represent the vorticity (perpendicular to the plane of measurements) which is clockwise for negative values and counterclockwise for positive values. Superimposed to these are arrows of the local velocity vectors shown every 7 vectors along the streamwise directions and every 5 along the normal direction. For these the modulus is square-rooted in order to magnify the size of the smaller vectors. The zero-velocity/vorticity area below the airfoil is not representative as this part of the field was not illuminated by the laser sheet. Similarly the thin, vertical vorticity bands below the airfoil's leading and trailing edges do not represent actual values of the vorticity but rather spurious values deriving from the velocity gradient between the illuminated and non-illuminated areas. Figure 8a) reveals that the magnitude of the boundary-layer vorticity at $\alpha = 7.5°$ decreases

more rapidly above the airfoil than at $\alpha = 10°$, Fig 8b). Furthermore it detaches from the trailing edge of the airfoil at $\alpha = 7.5°$ whereas it remains close to it at $\alpha = 10°$. This is more clearly visible in Fig. 9 which is an enlargement of the flow field close to the trailing edge. The same figure also shows that in this area the velocity vectors at $\alpha = 7.5°$ are smaller and less orderly oriented than those at $\alpha = 10°$. These findings suggest that an incipient flow separation may occur at the lower angle of attack. This appears consistent with the results from the balance measurements shown in Fig. 7 for the same conditions. Further investigation would be required to better understand the nature of this unexpected behavior, possibly resulting from larger vibration of the model at higher angles of attack.

Based on the experience with this initial model, new models will be designed to specifically test the benefit of changing the shape of airfoils by MFCs. First, baseline airfoils that have the potential of particularly benefit from this shaping technique will be selected. Then new models will be designed capable of displacing both the upper and the lower surfaces thus effectively producing a larger overall change of the airfoil shape. Finally, the models will be fabricated to allow significant shape changes starting closer to the leading edge (where the variations of the pressure coefficients and the effects on flow separation are typically larger).

IV. Conclusion

An airfoil model has been designed and constructed that has a flexible upper skin whose shape can be changed by macro fiber composite (MFC) actuators bonded to its inner side. These piezoelectric actuators are very thin, light, robust, and have low power consumption. In the design discussed they become an integral part of the upper skin of the model. Static actuation in still air at the minimum voltage of -500 V produces an outward displacement corresponding to 0.02 *c* whereas actuation at the maximum voltage of 1500 V produces an inward displacement corresponding to 0.03 *c*. Similar tests have been repeated in a wind tunnel at speeds up to 20 m/s and angles of attack up to 14°. In all cases the skin did not show any vibration or anomalous deformation and maintained a response to actuation comparable to that observed in still air. The aerodynamic characteristics of the airfoil have also been measured with a balance. The results obtained indicate that lower drag can be obtained for a given lift with deformation of the airfoil at some angles of attack. In other cases a lower pitching moment can be achieved. These results, obtained with a model not designed for optimizing the aerodynamic shape, suggest that the shaping of a surface by MFC actuators can be useful for tailoring the aerodynamic performance of an airfoil. In particular, this technique could be very beneficial to broaden and stabilize the useful aerodynamic-envelope characteristics of high-performance airfoils that quickly deteriorate at off-design conditions. Based on the experience with this initial model, new models will be designed to specifically test the aerodynamic benefits of changing the shape of airfoils by MFCs.

Acknowledgments

The authors would like to thank Mr. Thomas Ng Wenjie for preparing the preliminary power supply used to study the actuators and Mr. Fahad Ibn Azam, and Mr. Elayabharath Elango for their assistance with the experimental measurements.

References

[1] Reich, G. W., Bowman, J. C., and Sanders, B., "Large-Area Aerodynamic Control for High-Altitude Long- Endurance Sensor Platforms," *Journal of Aircraft* Vol. 42, No. 1, pp. 237.

[2] Maute, K. K., and Reich, G. W., "Integrated Multidisciplinary Topology Optimization Approach to Adaptive Wing Design," *Journal of Aircraft* Vol. 43, No. 1, pp. 253.

[3] Austin, F., Rossi, M. J., Van Nostrand, W., Knowles, G., and Jameson, A., "Static shape control for adaptive wings," *AIAA Journal* Vol. 32, No. 9, pp. 1895-1901.

[4] Laxminarayana Saggere, and Sridhar Kota, "Static Shape Control of Smart Structures Using Compliant Mechanisms ," *AIAA Journal* Vol. 37, No. 5, pp. 572.

[5] Secanell, M., Suleman, A, and Gamboa, P., "Design of a Morphing Airfoil Using Aerodynamic Shape Optimization," *AIAA Journal* , Vol. 44, No. 7, pp. 1550-1562.

[6] Siclari M. J., van Nostrand, W., and Austin, F., "The design of transonic airfoil sections for an adaptive wing concept using a stochastic optimization method," AIAA Paper 96-0329.

[7] Martins, A. L., and Catalano, F. M., "Drag optimization for transport aircraft Mission Adaptive Wing," *Journal of the Brazilian Society of Mechanical Sciences and Engineering* Vol. 25, No. 1, Jan./Mar. 2003.

[8] Hubbard, J. E. Jr., "Dynamic Shape Control of a Morphing Airfoil Using Spatially Distributed Transducers," *Journal of Guidance, Control, and Dynamics*, Vol. 29, No. 3, pp. 612-616.
[9] Munday, D., Jacob, J., and Huang, G., "Active Flow Control of Separation on a Wing with Oscillatory Camber," AIAA Paper 2002-0413, 40th AIAA Aerospace Sciences Meeting & Exhibit, Jan. 2002.
[10] Munday, D., and Jacob, J., "Active Control of Separation on a Wing with Oscillating Camber," *Journal of Aircraft*, Vol. 39, No. 1, 2002, pp. 187–189.
[11] Munday, D., Jacob, J., Hauser, T., and Huang, G., "Experimental and Numerical Investigation of Aerodynamic Flow Control Using Oscillating Adaptive Surfaces," AIAA Paper 2002-2837, 1st AIAA Flow Control Conference, June 2002.
[12] Ehlers, S. M., and Weisshaar, T.A., "Static aeroelastic control of an adaptive lifting surface," *Journal of Aircraft* Vol. 30, No. 4, pp. 534-540.
[13] Rocha, J., Moniz, P. A., Costa, A. P., and Suleman, A., "On Active Aeroelastic Control of an Adaptive Wing Using Piezoelectric Actuators," *Journal of Aircraft* Vol. 42, No. 1, pp. 278-281.
[14] Weisshaar, T. A., and Duke, D.K., "Induced Drag Reduction Using Aeroelastic Tailoring with Adaptive Control Surfaces," *Journal of Aircraft* Vol. 43, No. 1, pp. 157-164.
[15] Gern, F., Inman, D. J., and Kapania, R. K., "Computation of Actuation Power Requirements for Smart Wings with Morphing Airfoils," *AIAA Journal* Vol.43, No.12, pp. 2481-2486.
[16] Pinkerton, J. L., and Moses, R. W., "A Feasibility Study To Control Airfoil Shape Using THUNDER," NASA Technical Memorandum 4767.
[17] Bilgen, O., Kochersberger, K. B., Diggs, E. C., Kurdila, A. J., and Inman, D. J., "Morphing Wing Micro-Air-Vehicles via Macro-Fiber-Composite Actuators," AIAA Paper 2007-1785, *48th AIAA/ASME/ASCE/AHS/ASC Structures, Structural Dynamics, and Materials Conference*, Honolulu, Hawaii, Apr. 23-26, 2007.
[18] Bilgen, O., Kochersberger, K. B., Inman, D. J., and Ohanian, O. J. III, "Novel, Bidirectional, Variable-Camber Airfoil via Macro-Fiber Composite Actuators," *Journal of Aircraft* Vol. 47, No. 1, pp. 303-314.
[19] Moses, R. W., Pototzky, A. S., Henderson, D. A., Galea, S. C., Manokaran, D. S., Zimcik, D. G., et al., "Actively Controlling Buffet-Induced Excitations," report RTO-MP-AVT-123, Symposium on Flow Induced Unsteady Loads and the Impact on Military Applications, Apr. 2005.
[20] Jacobs, E. N., and Pinkerton, R. M., "Tests of the N.A.C.A. Airfoils in the Variable Density Wind Tunnel. Series 44 and 64," National Advisory Committee for Aeronautics technical note No. 401, Dec. 1931.

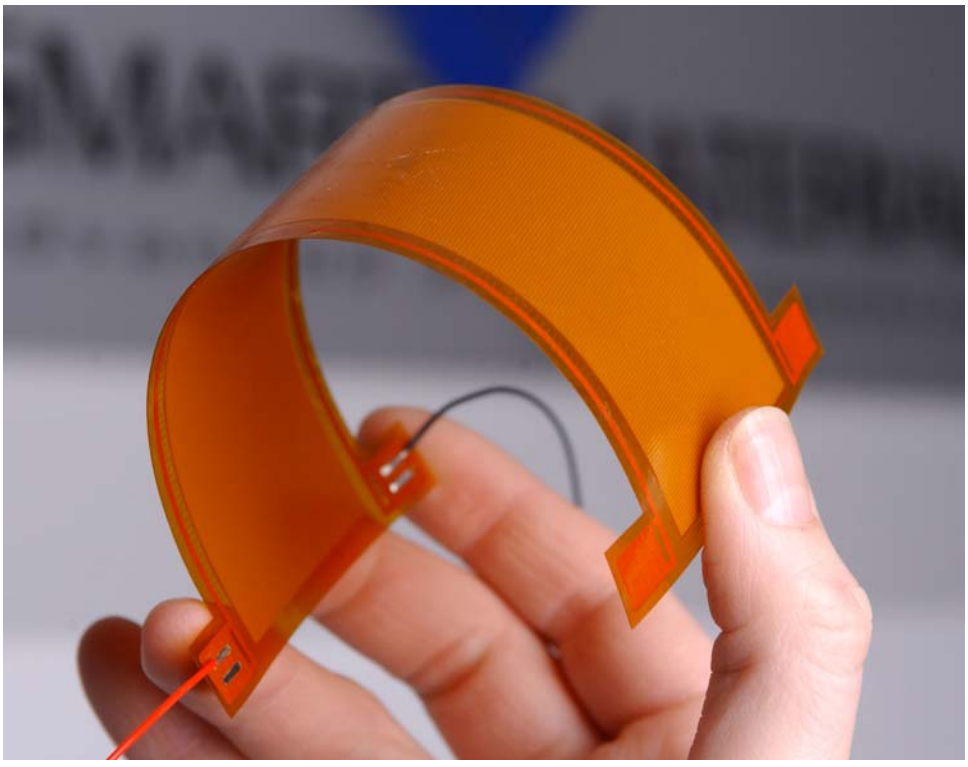

Figure 1. Macro fiber composite (MFC) actuator [image courtesy of Smart Material Corp.].

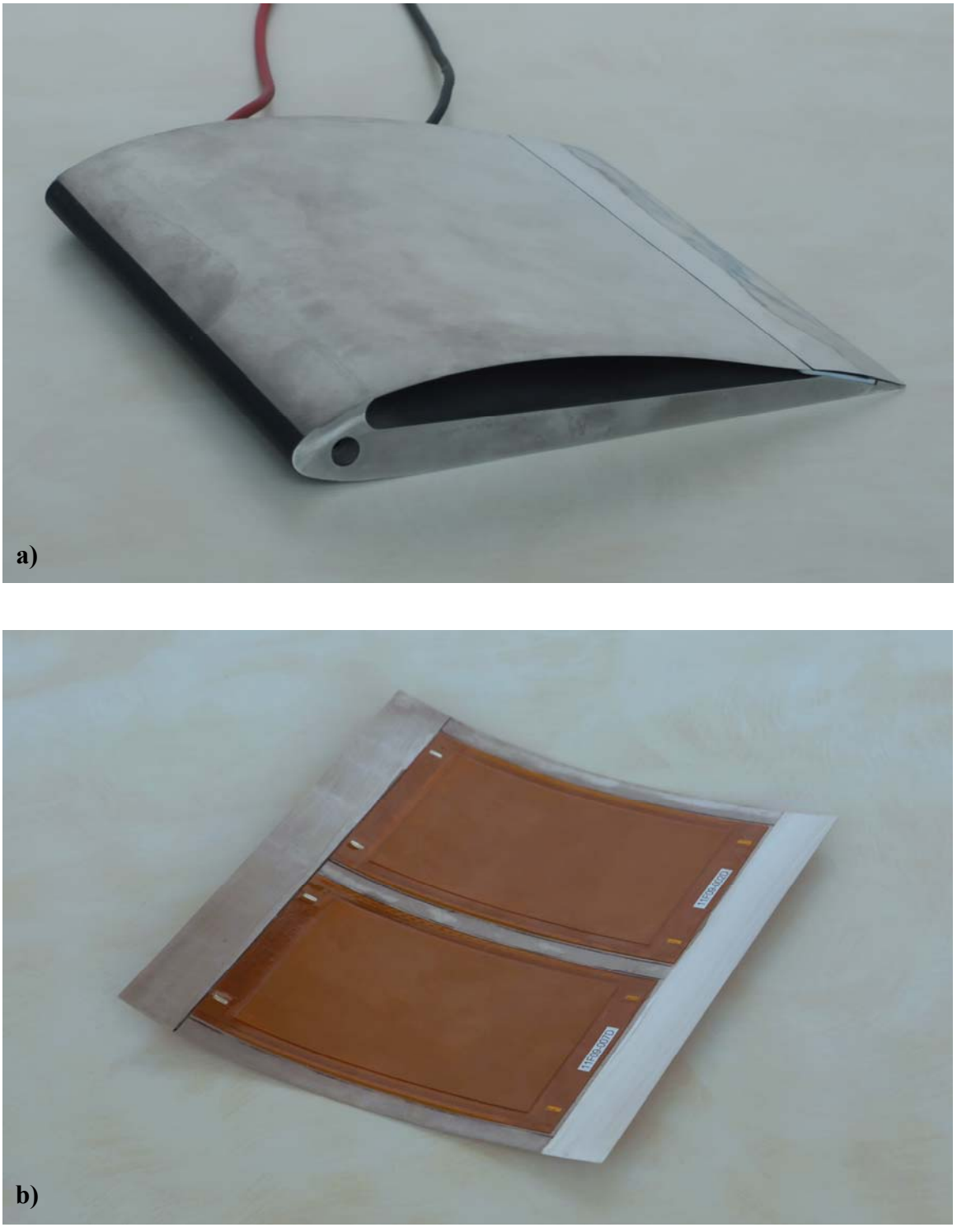

Figure 2. Airfoil model for testing: a) assembled model; b) inner side of the upper skin with MFC patches.

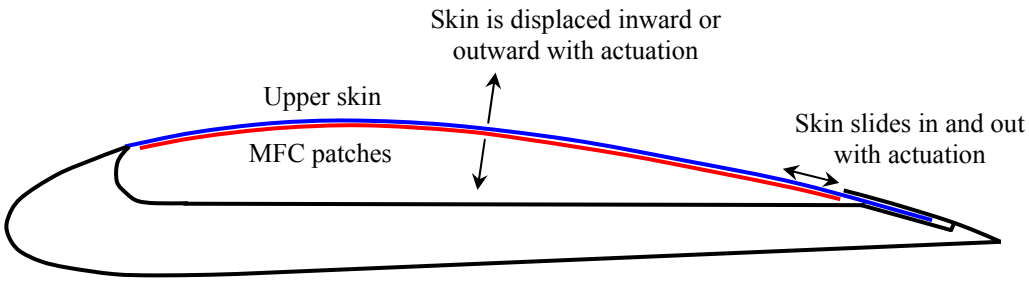

Figure 3. Schematic diagram of upper-surface actuation by MFC patches.

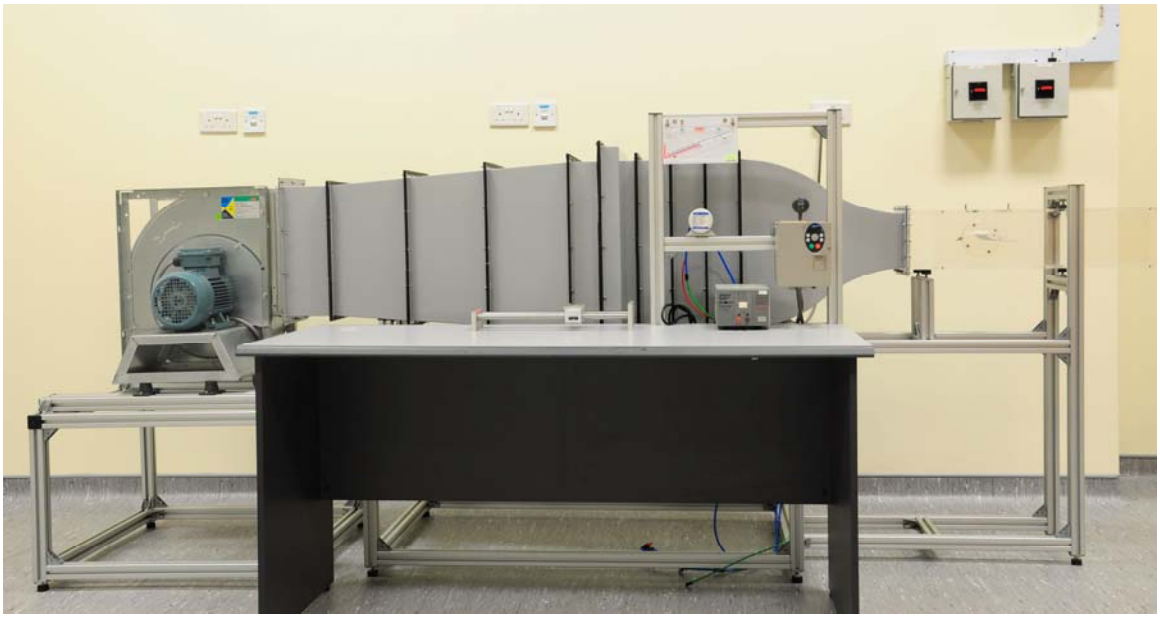

Figure 4. Small, open-loop, subsonic wind tunnel of the NUS Temasek Laboratories.

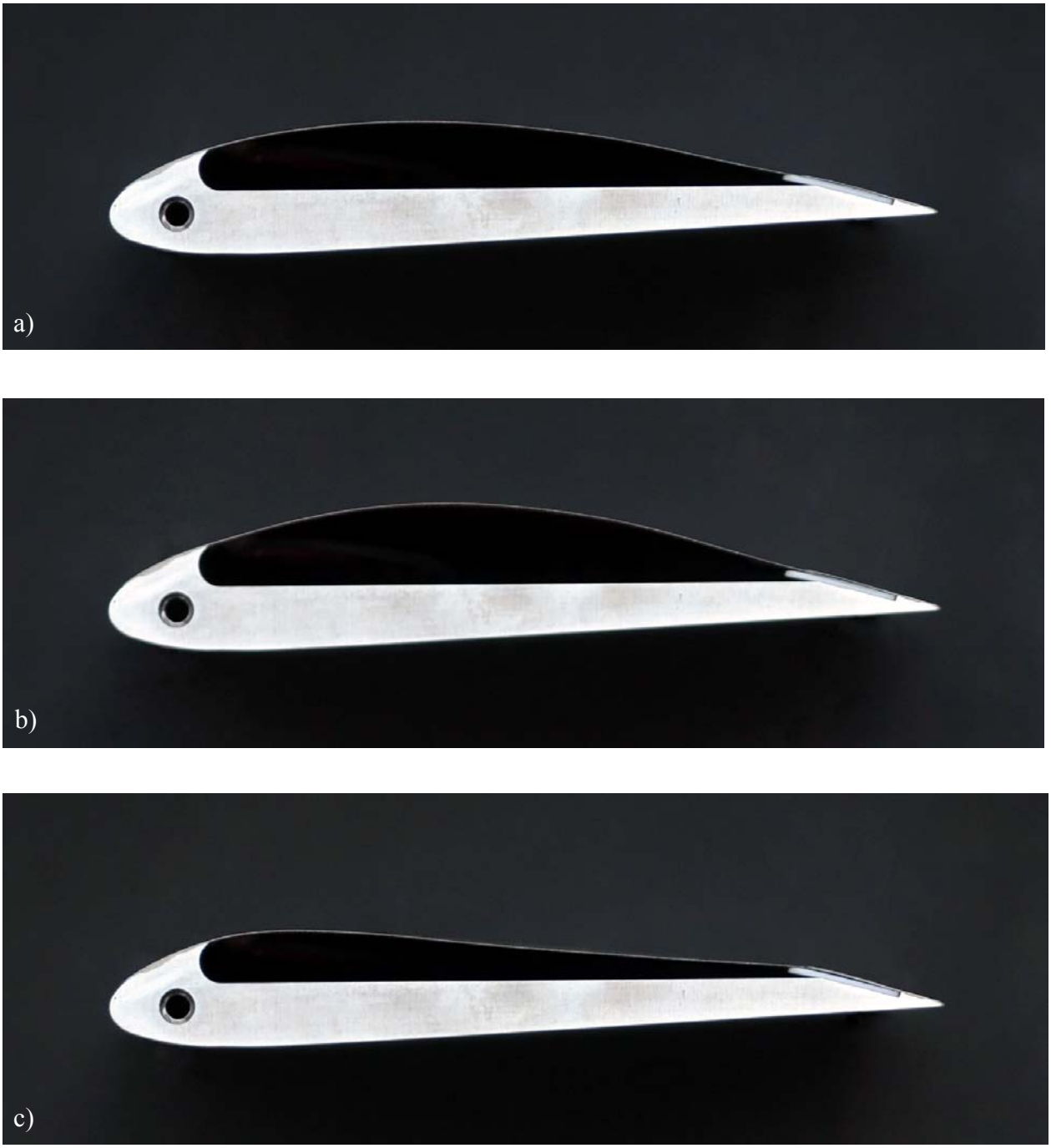

Figure 5. Lateral view of the airfoil model: a) without actuation (shape similar to the NACA 4415 airfoil); b) with actuation at -500 V (3 mm maximum outward displacement); c) with actuation at 1500 V (5 mm maximum inward displacement).

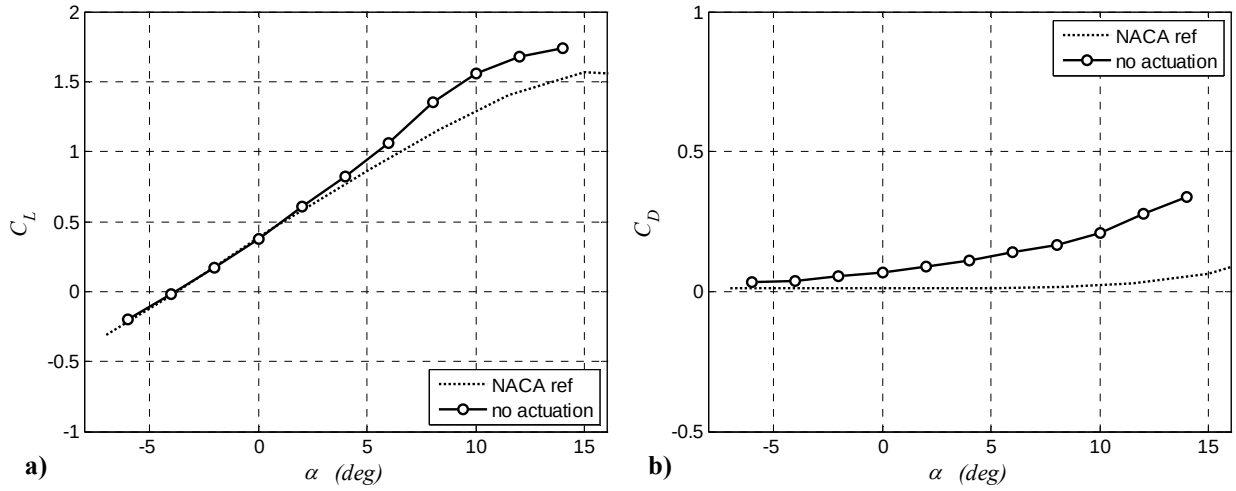

Figure 6. Comparison of NACA 4415 airfoil[19] and non-actuated model: a) lift coefficient; b) drag coefficient.

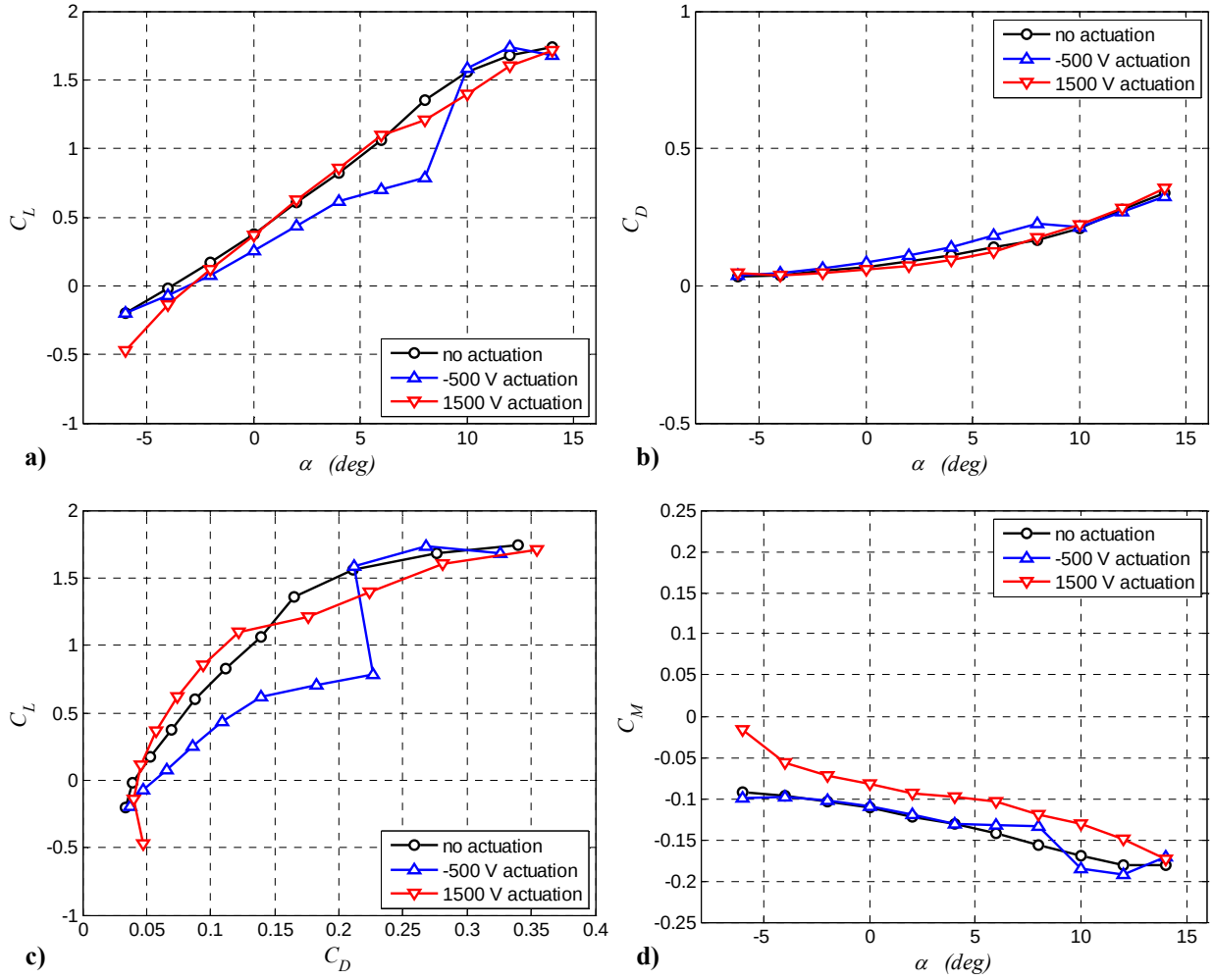

Figure 7. Aerodynamic characteristics of the airfoil model without and with actuation: a) lift coefficient; b) drag coefficient; c) lift-drag polar; d) pitching moment about *c*/4.

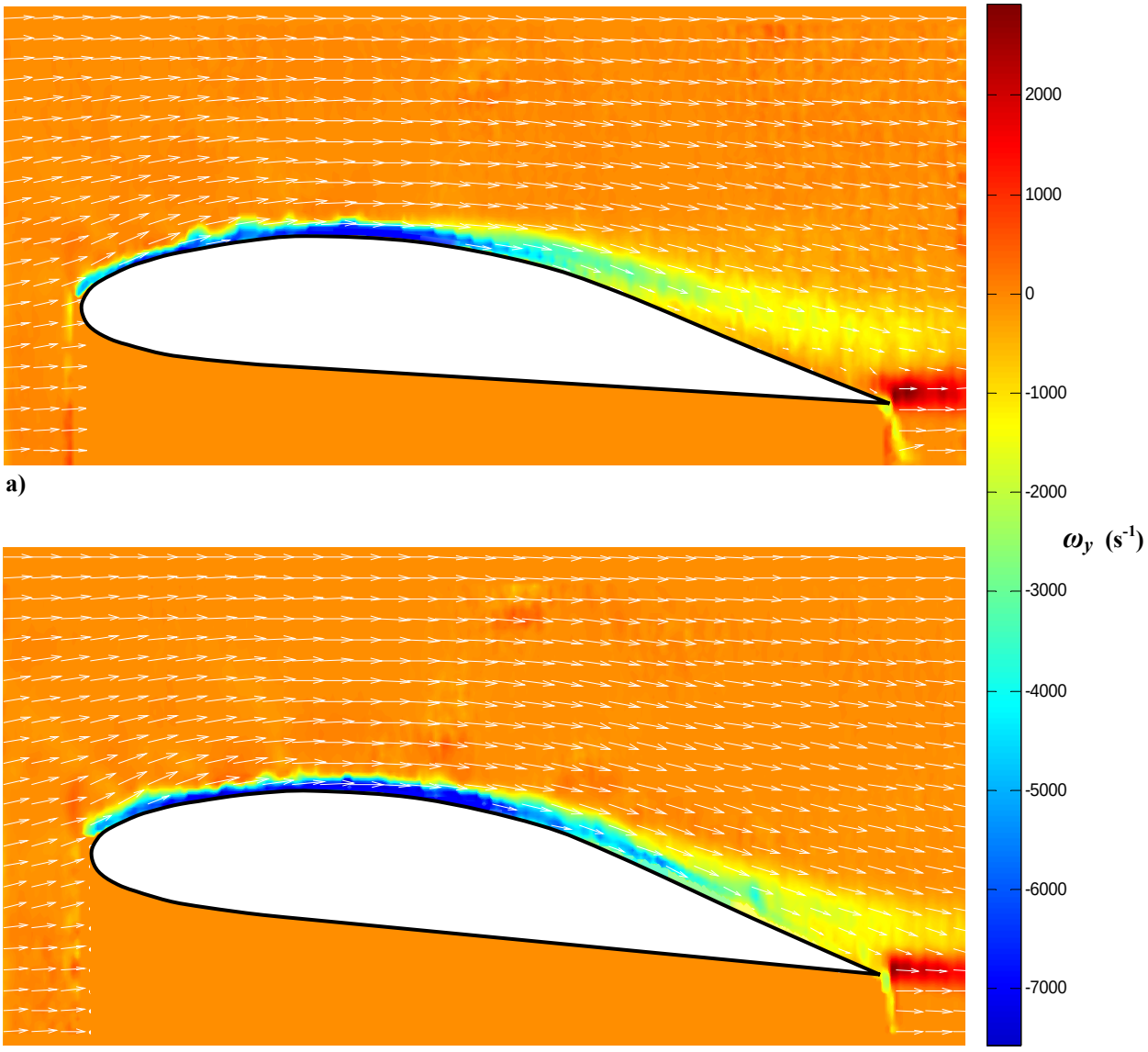

Figure 8. Flow fields above the model actuated at -500 V from PIV measurements at U_∞ = 15 m/s : a) α = 7.5°; b) α = 10°. The color field represents the values of the vorticity, the arrows indicate the local velocity vectors.

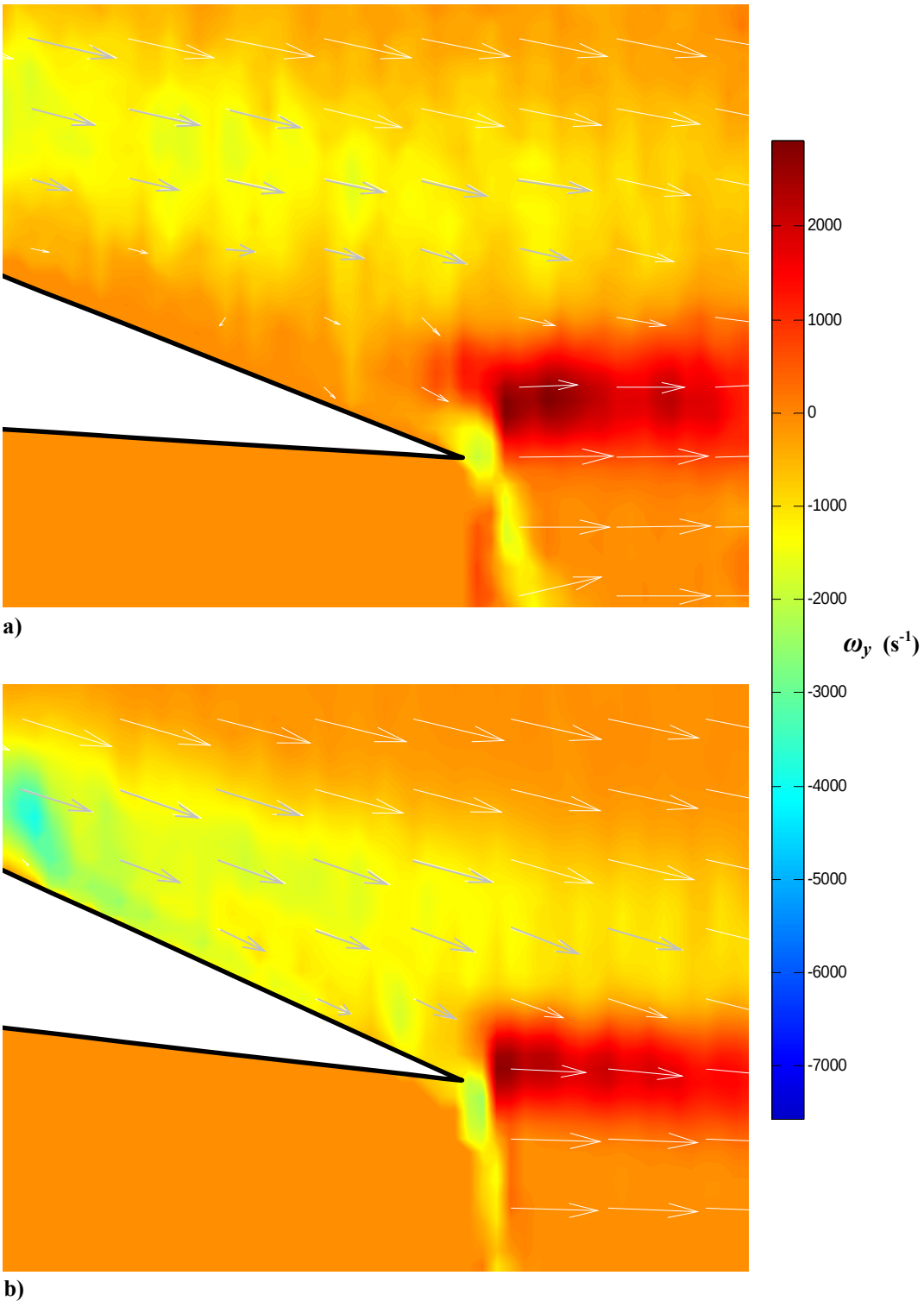

Figure 9. Enlargement of the flow fields around the trailing-edge area of the model actuated at -500 V from PIV measurements at U_∞ = 15 m/s : a) α = 7.5°; b) α = 10°. The color field represents the values of the vorticity, the arrows indicate the local velocity vectors.